Supplementary Figures

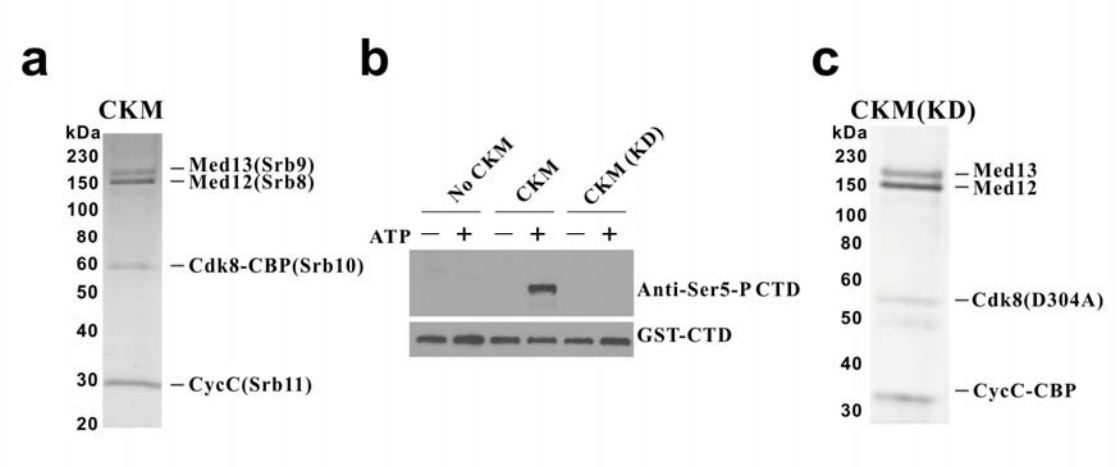

Supplementary Figure 1. Purification of yeast CKM. (**a**) Silver-stained SDS-PAGE analysis of CKM purified through a TAP-tag engineered into the Cdk8 C-terminus. (**b**) Kinase activity of wild-type and mutant (D304A mutation in the Cdk8 kinase eliminates its kinase activity) CKMs on the Ser5 residue of the RNAPII CTD. In the GST-CTD, the RNAPII CTD was fused to the C-terminus of GST. (**c**) The kinase-dead (KD) CKM bearing a D304A mutation was also purified from yeast cells using the TAP method.

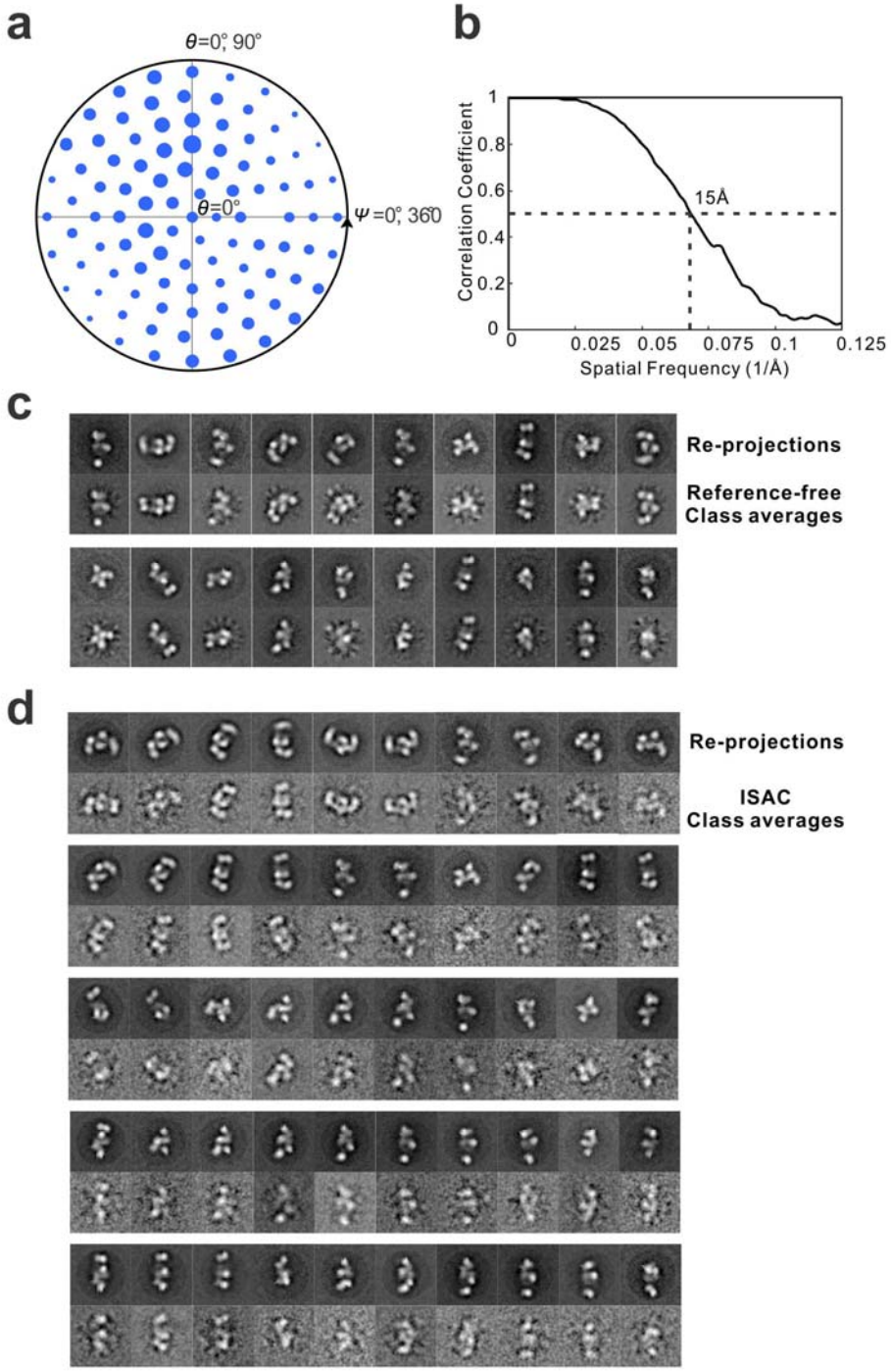

Supplementary Figure 2. Angular coverage, resolution, and validation of the yeast CKM cryo-EM map. (**a**) Angular distribution plot (in polar coordinates, with θ plotted outward from the origin and Ψ along the circumference) showing the

distribution of orientations for CKM single particle images used for calculation of the 3D map. (**b**) Fourier Shell Correlation (FSC) curve for the cryo-EM map of the CKM. Using a FSC = 0.5 criterion, the resolution of the map is estimated to be ~15 Å. (**c**) Re-projections of the CKM cryo-EM map are shown above and compared to corresponding class averages obtained by reference-free alignment of particles assigned to the Euler group represented by the projection. The similarity between each projection and the corresponding class average suggests that the CKM cryo-EM reconstruction accurately represents the structure of the CKM. (**d**) In a more rigorous test of the CKM cryo-EM map, re-projections of the CKM cryo-EM map are shown above and compared to class averages obtained by analyzing CKM cryo-images using an Iterative Stable Alignment and Clustering (ISAC) algorithm that clusters and aligns images without any reference to the CKM cryo-EM map.

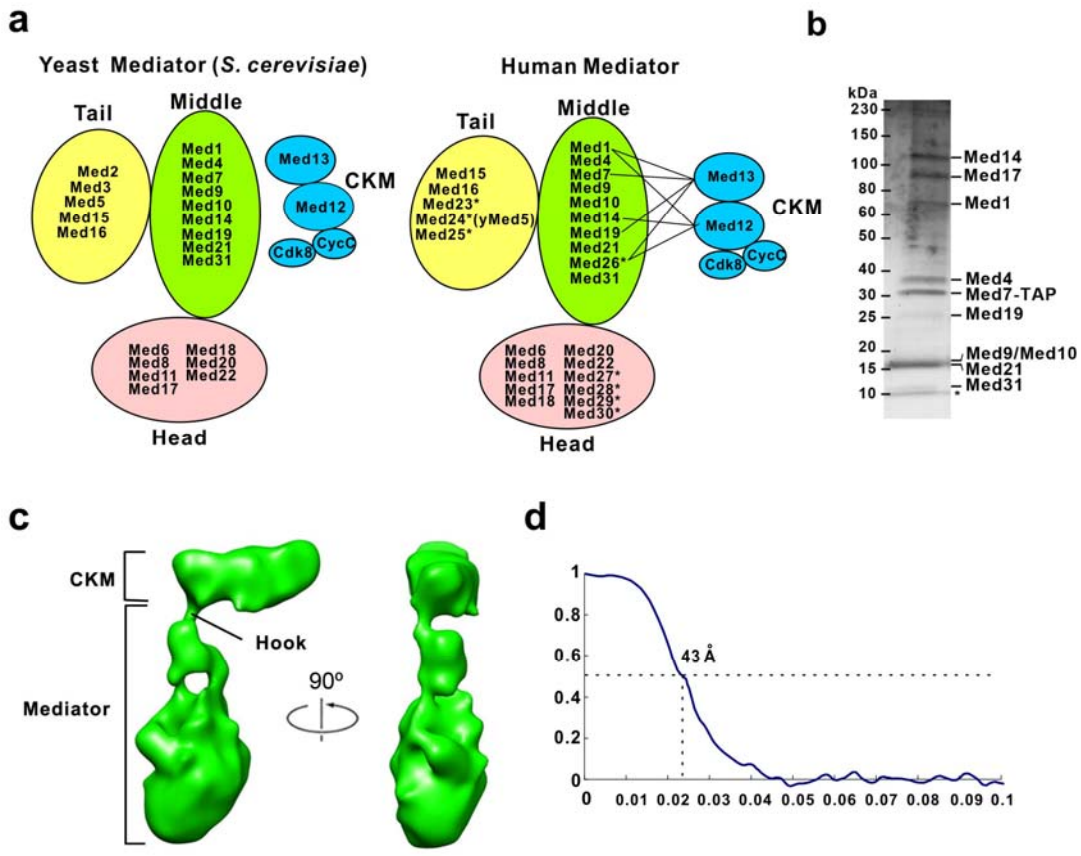

Supplementary Figure 3. Yeast and human Mediator module subunit composition, SDS-PAGE analysis of a purified yeast Middle module, and a 3D EM map of the human Mediator–CKM complex. (**a**) Subunit composition of the Head, Middle, and Tail, modules of the yeast and human Mediator complexes. The names of human Mediator subunits not present in yeast Mediator are marked by asterisks. (**b**) Silver-stained SDS-PAGE analysis of Middle module purified from a ΔMed16 deletion strain with a TAP-tag engineered into the Med7 C-terminus. A band marked with an asterisk near the bottom of the gel is the gel dye front. (**c**) Human Mediator–CKM 3D EM map. (**d**) FSC plot used to estimate the resolution of the Human Mediator–CKM map at ~40Å.

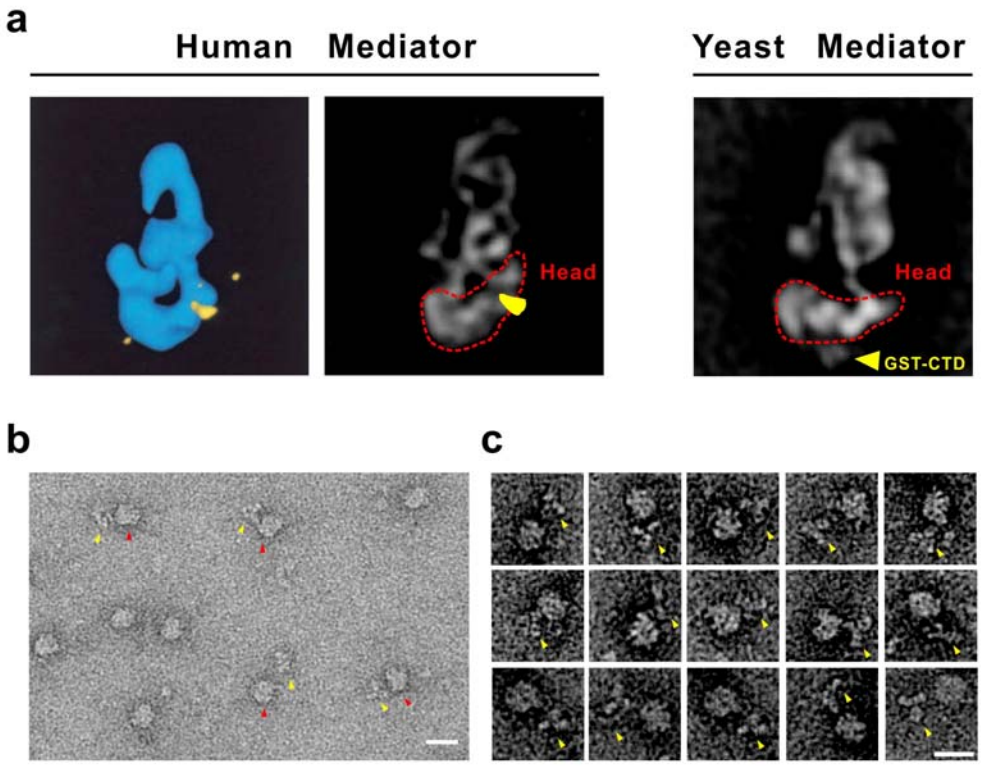

Supplementary Figure 4. Localization of a reported CTD-binding site on human Mediator to the Head module, and antibody labeling of the RNAPII CTD. (**a**) Comparison of a published image showing the position for CTD binding to human Mediator (left) with 2D class averages obtained from human Mediator particles (middle) and yeast GST-CTD bound Mediator particles (right) indicates that the previously reported position for CTD binding is on the Head module of human Mediator. (**b**) A micrograph showing RNAPII particles with their CTDs labeled with an antibody targeting a calmodulin-binding peptide (CBP)-tag at the C-terminal end of the CTD (Genscript, A00635). After incubation with anti-CBP antibody, labeled RNAPII particles were purified through a heparin column to remove unbound antibodies. Bound antibodies are close to the main body of RNAPII, suggesting that the end of the CTD lies near the RNAPII. This is indicative of a compact conformation of the unphosphorylated CTD. RNAPII and antibody particles are indicated with red and yellow arrows, respectively. (**c**) Raw individual particle images showing the end of the CTD close to the RNAPII. Scale bar represents 20 nm.

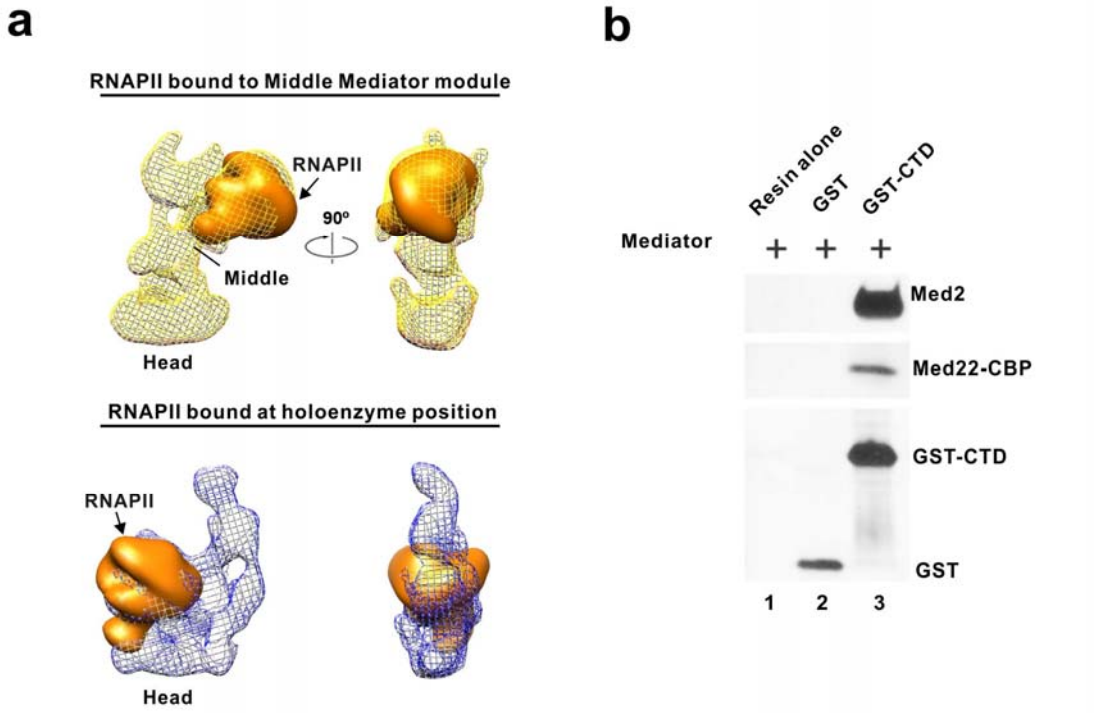

Supplementary Figure 5. RNAPII and CTD interaction with Mediator. (**a**) 3D EM maps showing RNAPII (colored in orange) bound to the Middle Mediator module (top), and near the Head module in the Mediator–RNAPII holoenzyme. (**b**) A GST pull-down assay was used to analyze the interactions between Mediator and the RNAPII CTD. GST (lane 2) or GST-CTD (lane 3) was immobilized on glutathione-agarose resin and incubated with Mediator at 4°C for 4h. After washing three times, bound proteins were eluted by mixing the resin with 25 μl SDS-PAGE loading buffer. Mediator binding was probed by western blotting using antibodies against Med2 (Santa Cruz, sc-28058) or the CBP-tag at the Med22 C-terminus (Genscript, A00635). The GST and GST-CTD were detected using an anti-GST antibody (Genscript, A00865). The results illustrate how Mediator interacts with the GST-CTD, but not with GST alone.

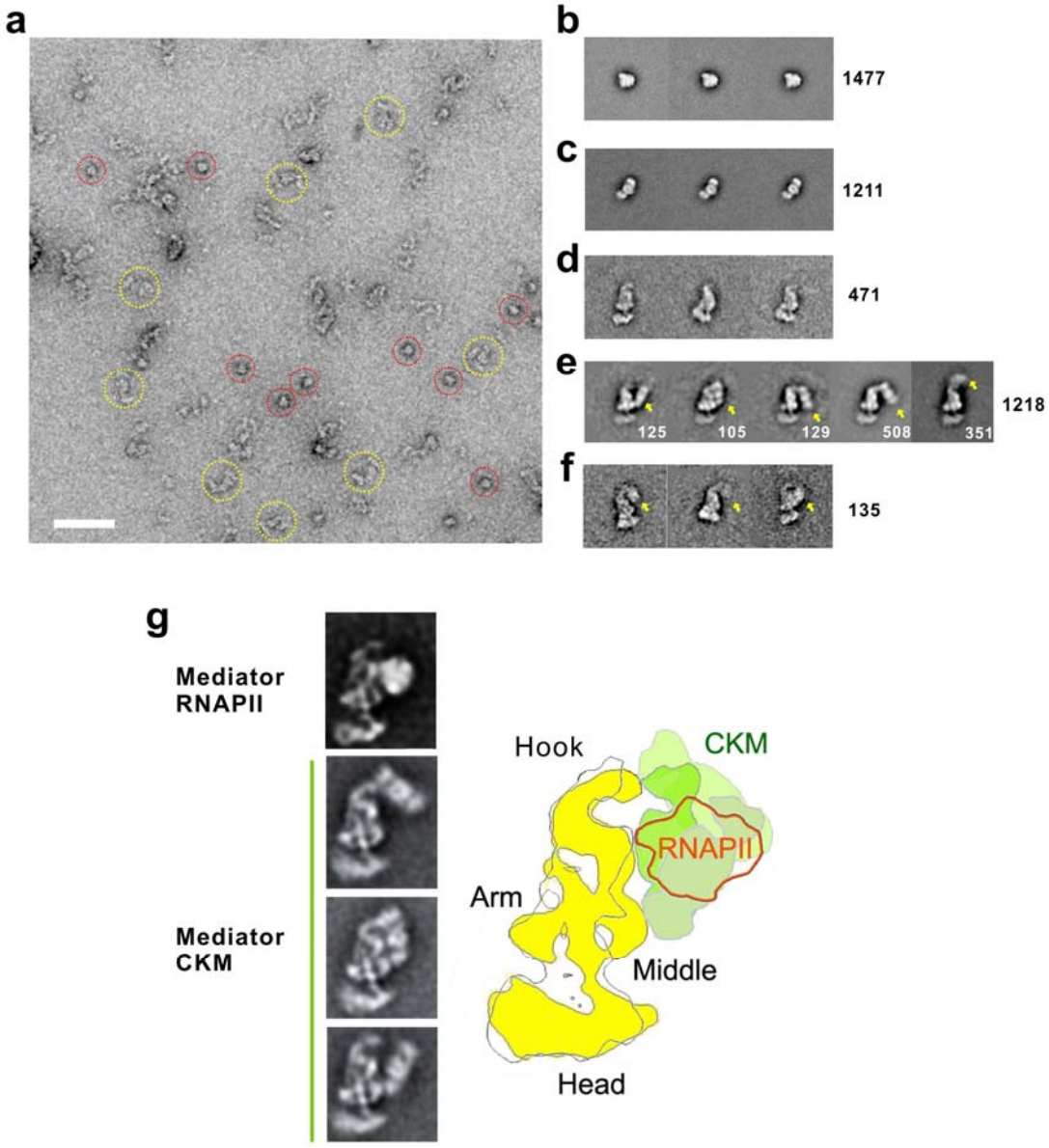

Supplementary Figure 6. CKM inhibits binding of RNAPII to Mediator. (**a**) Micrograph of the Mediator incubated with RNAPII and CKM. RNAPII and Mediator-CKM particles are boxed with yellow and red dashed circles, respectively. (**b**) RNAPII class averages. (**c**) CKM class averages. (**d**) Mediator class averages. (**e**) Mediator–CKM class averages, with CKM density highlighted by the yellow arrows heads. The number of particles in each class is shown. (**f**) Mediator–RNAPII class averages. No

Mediator-CKM-RNAPII ternary complexes were found. The scale bar represents 100 nm and the numbers on the right indicate the total number of particles for each type of complex. (**g**) EM class averages (left) show interaction of RNAPII and the CKM with the Middle module, and a diagram (right) illustrates how binding positions for the CKM overlap with the position that would be occupied by RNAPII after CTD-dependent interaction with the Middle module.

Supplementary Table 1. *S. cerevisiae* strains used in this study

Strain	Genotype	Source
BJ2168	*MATa leu2 trp1 ura3-52 prb1-1122 pep4-3 prc1-407 gal2*	ATCC
KTA312	*BJ2168, CycC-TAP::KlTRP1 med13Δ::KanMX6*	This study
KTA315	*BJ2168, CycC-TAP::KlTRP1 Cdk8$^{(473\text{-}555)\ \Delta}$::KanMX6*	This study
KTA317	*BJ2168, CycC-TAP:: KlTRP1 Cdk8$^{(D304A)}$::KanMX6*	This study
KTA318	*BJ2168, CycC-TAP::KlTRP1 MED12$^{(375\text{-}1427)\ \Delta}$::KanMX6*	This study
KTA401	*BJ2168, Med22-TAP::KlTRP1*	This study
KTA403	*BJ2168, Med22-TAP::KlTRP1 Med18-FLAG::KanMX6*	This study
KTA405	*BJ2168, Med22-TAP::KlTRP1 Med16-FLAG::KanMX6*	This study
KTA407	*BJ2168, Med16-MBP-ProA::KanMX6*	This study
CA001	*BJ2168, Med22-10xHis-ProA::KlTRP1, Med8- PreSci-3xHA::Kan*	(ref. 5)
KTA501	*BJ2168, RPB1-TAP::KlTRP1*	This study
KTA502	*BJ2168, Med7-TAP::KlTRP1 med16Δ::KanMX6*	This study
Z695	*MATa ura3-52 his3Δ200 leu2-3, 112 rpb1Δ187::HIS3 srb8-1 [pC6(LEU2 rpb1Δ104)]*	(ref. 13)
Z735	*MATa his3Δ200 leu2-3, 112 ura3-52 rpb1Δ187::HIS3 srb10-1 (AMP, URA3, CEN, RPB1+)*	(ref. 7)

Supplementary Note

Testing the kinase activity of purified yeast CKM: To test the functionality of the purified CKM we performed assays to monitor the reported kinase activity of the CKM on the CTD. We found that our purified wild-type CKM was able to phosphorylate a recombinant GST-tagged CTD (**Supplementary Fig. 1b**). A mutant CKM bearing a Cdk8 D304A point mutation could be purified as an intact complex but had no CTD kinase activity (**Supplementary Fig. 1c**).

Calculation of a yeast CKM cryo-EM map: To overcome problems associated with stain-induced preservation, and to better understand the structure of the CKM, we calculated a 3D map of the CKM from images of CKM particles preserved in amorphous ice. We low-pass filtered (to ~50 Å) the CKM volume calculated from stained specimens and used it as an initial reference for iterative refinement of alignment parameters for ~70,000 CKM cryo-images. The angular distribution of images in the cryo-EM data set indicated that an adequate number of CKM particle orientations were recorded and analyzed (**Supplementary Fig. 2a)**, and the CKM cryo-EM map showed the structure of the complex free of specimen preservation artifacts (**Fig. 1c**), at an estimated resolution of ~15 Å (0.5 Fourier shell correlation criterion; **Supplementary Fig. 2b**). Class averages obtained by reference-free alignment within groups of cryo-EM images segregated by orientation showed good agreement with projections of the CKM cryo-EM volume (**Supplementary Fig. 2c**). Additional evidence to support the correctness of the CKM cryo-EM map came from the close correspondence between projections of the CKM cryo-EM volume and class averages independently obtained using an iterative alignment and clustering algorithm (ISAC)[1] (**Supplementary Fig. 2d**).

3D EM maps of the Mediator–CKM complex: To arrive at a more complete understanding of the interaction between Mediator and the CKM we used the

Random Conical Tilt method[2] to calculate 3D EM maps of yeast Mediator–CKM complexes. Zero-tilt images of yeast Mediator–CKM particles were clustered into homogeneous groups showing the same Mediator–CKM interaction and corresponding tilted images were used to calculate 3D maps. We obtained 3D maps showing the strong (Mediator) hook–Med13 interaction, or an extended Mediator–CKM interface (**Fig. 2f**). The resolution of these maps was limited to ~35Å**,** but fitting cryo-EM maps of yeast Mediator[3] and the CKM showed that the maps from stained particle images were free of major deformation artifacts and provided a detailed 3D view of the yeast Mediator–CKM interaction (**Fig. 2g**).

Possible mechanism of CKM transcription repression: A study of the Mediator–CKM interaction in *S. pombe* concluded that repression resulted from direct blocking of the RNAPII binding site by the CKM[4]. In contrast, biochemical and EM analyses of the human Mediator–CKM interaction detected no overlap between the locations for CKM and RNAPII binding to Mediator. This observation, along with consideration of a previous report indicating that binding of the CKM and RNAPII to Mediator were mutually incompatible[5], led to the suggestion that the CKM might prevent RNAPII binding by inducing a Mediator conformation incompatible with RNAPII interaction[6]. However, no direct evidence to support this interpretation was provided.

No large changes in conformation are apparent in 2D or 3D maps of yeast Mediator upon CKM binding (see **Fig. 2c and f**). This seems reasonable because the main Mediator–CKM contact involves the highly mobile hook, whose conformation appears uncorrelated to the conformation of other portions of the yeast Mediator structure[3]. An effect of the CKM interaction on Mediator conformation as an explanation for CKM repression would not account for the fact that all CKM components bear SRB mutations that reflect a strong genetic connection to the RNAPII CTD, which in turn is critically involved in Mediator–RNAPII interaction and holoenzyme formation[7,8]. On the other hand, it has been reported that CKM binding to human Mediator abolishes a strong interaction with the RNAPII CTD observed for

Mediator alone[5], which would support our hypothesis of CKM repression through inhibition of CTD-dependent RNAPII interaction with Mediator.

Supplementary Video Legends

Supplementary Video 1. A movie illustrating the different orientations of Mediator-bound CKM. The animation was assembled from 89 class averages obtained by clustering of Mediator-CKM images. Each class average resulted from alignment of about 40 single-particle images. The class averages were aligned using Mediator as a reference and then sorted according to the different orientations of CKM. The movie shows that the CKM can occupy different positions around the back and top of Mediator, in an interaction dictated by contacts between the CKM and two areas of Mediator, one in the Mediator Middle module, and a second one at the distal end of the hook at the end of the Mediator Tail module.

Supplementary Video 2. A movie illustrating the CTD-dependent interaction of RNAPII with Mediator. The animation was assembled from 19 class averages obtained by clustering of Mediator-RNAPII images. Each class average resulted from alignment of about 25 single-particle images. The class averages were aligned using Mediator as a reference and then sorted according to the different positions of RNAPII. The movie shows that RNAPII can occupy different positions around the back and top of Mediator.

Supplementary References

1. Yang, Z., Fang, J., Chittuluru, J., Asturias, F.J. & Penczek, P.A. Iterative Stable Alignment and Clustering of 2D Transmission Electron Microscope Images. *Structure* **20**, 237-247 (2012).
2. Radermacher, M. The three-dimensional reconstruction of single particles from random and non-random tilt series. *J. Electron Microsc. Tech.* **9**, 359-394 (1988).

3. Cai, G., Imasaki, T., Takagi, Y. & Asturias, F.J. Mediator structural conservation and implications for the regulation mechanism. *Structure* **17**, 559-567 (2009).
4. Elmlund, H.*, et al.* The cyclin-dependent kinase 8 module sterically blocks Mediator interactions with RNA polymerase II. *Proc Natl Acad Sci U S A* **103**, 15788-15793 (2006).
5. Naar, A.M., Taatjes, D.J., Zhai, W., Nogales, E. & Tjian, R. Human CRSP interacts with RNA polymerase II CTD and adopts a specific CTD-bound conformation. *Genes Dev* **16**, 1339-1344 (2002).
6. Knuesel, M.T., Meyer, K.D., Bernecky, C. & Taatjes, D.J. The human CDK8 subcomplex is a molecular switch that controls Mediator coactivator function. *Genes Dev* **23**, 439-451 (2009).
7. Nonet, M.L. & Young, R.A. Intragenic and extragenic suppressors of mutations in the heptapeptide repeat domain of Saccharomyces cerevisiae RNA polymerase II. *Genetics* **123**, 715-724 (1989).
8. Svejstrup, J.Q.*, et al.* Evidence for a mediator cycle at the initiation of transcription. *Proc. Natl. Acad. Sci.* **94**, 6075-6078 (1997).